doi:10.4149/gpb_2011_01_100

Short Communication

Pharmacological studies of $Ca_V3.1$ T-type calcium channels using automated patch-clamp techniques

Kee-Hyun Choi, Chiman Song, Chan S. Cheong and Hyewhon Rhim

Life/Health Division, Korea Institute of Science and Technology, 39-1 Hawolgok-Dong, Seongbuk-Gu, Seoul, Korea

Abstract. T-type calcium channels are involved in a variety of physiological and pathophysiological processes, and thus could be therapeutic targets. However, there is no T-type channel selective blocker for use in clinical practice, demanding a need for the development of novel drugs where a higher-throughput screening system is required. Here we present pharmacological studies on $Ca_V3.1$ T-type channels using automated patch-clamp. The IC_{50} values obtained from automated patch-clamp and conventional one showed a good correlation (correlation coefficient of 0.82), suggesting that the automated patch-clamp is an efficient and reliable method for ranking the drug potencies for T-type channels.

Key words: T-type calcium channel — $Ca_V3.1$ — Automated patch-clamp — Drug discovery

T-type calcium channels are present in nerve tissues, heart, smooth and skeletal muscles, and endocrine tissues, involved in neuronal excitability, cardiac pacemaker activity, smooth muscle contraction and hormone secretion (Perez-Reyes 2003). Neuronal T-type calcium channels in particular have been suggested to play a vital role in regulation of sleep (Anderson et al. 2005), nociception (Kim et al. 2003), epilepsy (Tsakiridou et al. 1995) and neuropathic pain (McCallum et al. 2003), thus becoming an attractive target for such disorders. Indeed, T-type calcium channel blockers have been demonstrated to be effective for treatment of cerebral diseases such as absence epilepsy (Vitko et al. 2005), epilepsy (Khosravani et al. 2005) and neuropathic pain (Flatters 2005). Mibefradil, a specific blocker of T-type calcium channels had been used for therapeutic treatment of hypertension and angina pectoris (Clozel et al. 1990). However, mibefradil is metabolized by cytochromes P450 3A4 and 2D6 with other drugs and interacts with them pharmacokinetically, which results in various adverse effects including irregular heart rhythms (Krayenbuhl et al. 1999). As a result, mibefradil has been withdrawn from the market so that a selective blocker for T-type calcium channels for clinical use is not available, waiting for the development of T-type calcium channel specific drugs.

For ion channel drug discovery, patch-clamp measurements have been the gold-standard assay. However, the conventional patch-clamp is not suitable for effective screening in early stages of drug discovery due to its time-consuming and labor-intensive nature. Recent developments of automated patch-clamp devices are rapidly utilized for ion channel drug discovery as well as safety pharmacology such as cardiac toxicity tests using hERG channels (Dunlop et al. 2008). Numerous research papers on assessments of cardiac hERG channel liability with various automated patch-clamp devices have been reported (Bridgland-Taylor et al. 2006; Ly et al. 2007), revealing that the automated patch-clamp is reliable for ranking the potencies of drugs. However, T-type calcium channels have not been rigorously tested using automated patch-clamp except for a brief case study on $Ca_V3.2$ T-type calcium channels (Mathes et al. 2009). Thus, pharmacological studies on T-type calcium channels with automated patch-clamp would be valuable due to urgent needs for developments of T-type calcium channel specific drugs for clinical use. In the present work, recombinant $Ca_V3.1$ T-type calcium channels were studied using auto-

Electronic supplementary material. Detailed experimental procedures, additional results, discussion, Figures S1–S8 and Table S1. The online version of this article (doi:10.4149/gpb_2011_01_100) contains supplementary material, which is available to authorized users.

Correspondence to: Kee-Hyun Choi and Hyewhon Rhim, Life/Health Division, Korea Institute of Science and Technology, 39-1 Hawolgok-Dong, Seongbuk-Gu, Seoul 136-791, Korea
E-mail: keehyun@kist.re.kr
hrhim@kist.re.kr

mated patch-clamp, where four independent patch-clamp measurements can be conducted in parallel.

To characterize pharmacological properties of $Ca_v3.1$ T-type calcium channels, whole-cell currents were recorded from HEK293 cells stably expressing $Ca_v3.1$ channels with automated patch-clamp. Mibefradil, the best-known T-type calcium channel specific blocker (Martin et al. 2000) was initially tested. The effects of mibefradil on $Ca_v3.1$ chan-

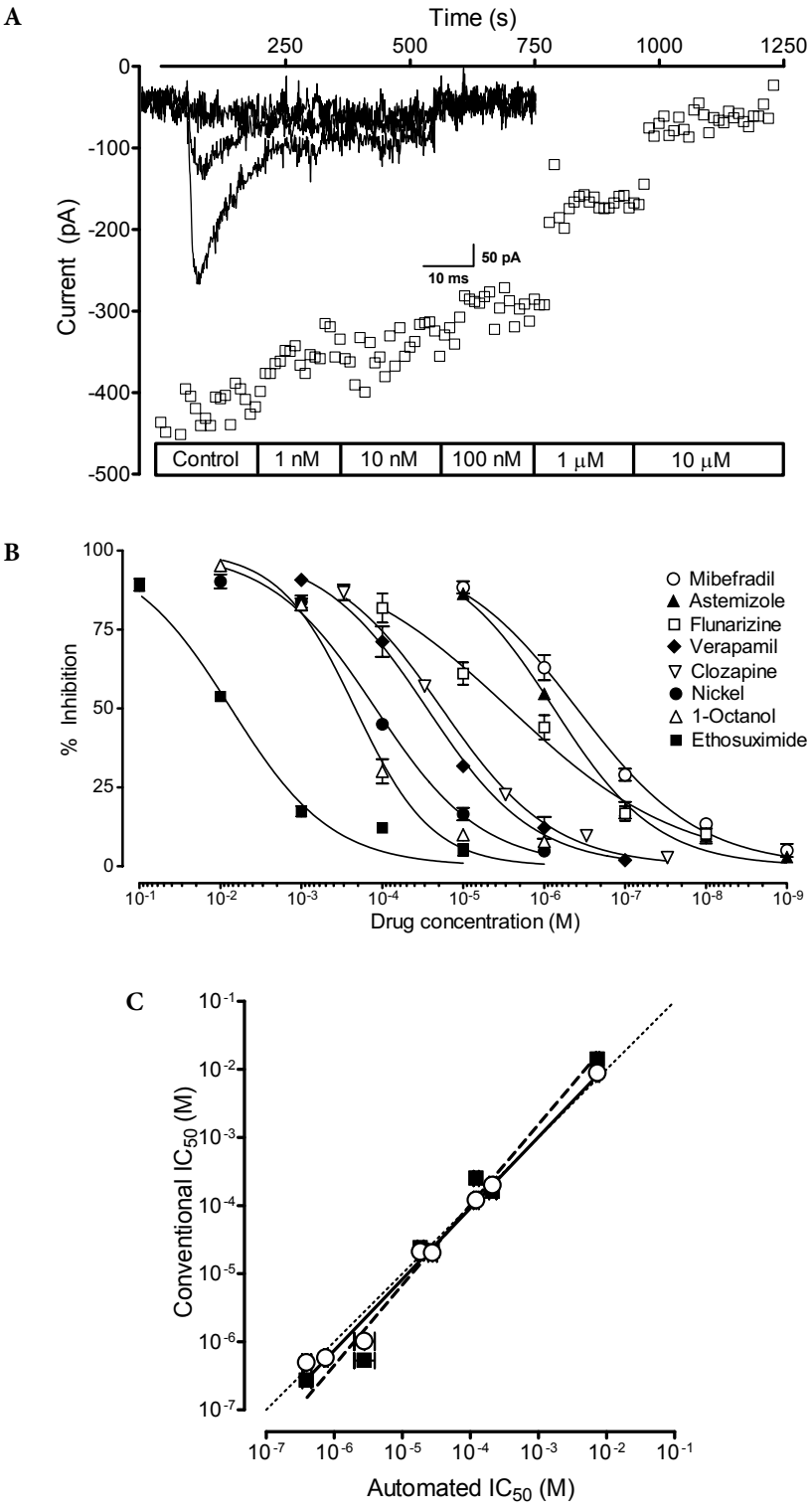

Figure 1. Pharmacological characterization of $Ca_v3.1$ channels with automated patch-clamp. **A.** Mibefradil inhibition of $Ca_v3.1$ channels was tested in automated patch-clamp. Time course of the amplitude of the peak $Ca_v3.1$ currents in response to increasing concentrations of mibefradil of 1 nM, 10 nM, 100 nM, 1 μM and 10 μM as shown at the bottom. Insert: A representative whole-cell recording of $Ca_v3.1$ channels evoked by 50-ms test pulses to –20 mV at a holding potential of –100 mV. Whole-cell currents of $Ca_v3.1$ channels were blocked by ~60% on average upon applying 1 μM mibefradil to the bath solution (control, 1 μM and 10 μM of mibefradil applied). **B.** Dose-response curves of drug inhibition of the peak $Ca_v3.1$ currents presented as percent inhibition (% inhibition) as a function of drug concentration: mibefradil (○), astemizole (▲), flunarizine (□), verapamil (◆), clozapine (▽), nickel (●), 1-octanol (△) and ethosuximide (■). Each point is pooled from at least five recordings. The curves were fitted to a Hill equation to obtain the IC_{50} values, summarized in Table 1. Error bars represent S.E.M. **C.** Comparison of the potencies of T-type calcium channel blockers obtained with automated and conventional patch-clamps. The IC_{50} values determined in automated patch-clamp were plotted against those obtained with conventional patch-clamp in the present study (open circles) as well as in the literature (filled squares). The solid line indicates a linear regression with the values measured in the present experiments (slope = 0.96 ± 0.05, correlation coefficient, $R = 0.82$), and the dashed line indicates a linear regression with the literature values (slope = 0.85 ± 0.09, $R = 0.70$). Unity is represented as a dotted line. Error bars represent S.E.M.

Table 1. Summary of the pharmacological studies of $Ca_v3.1$ channels obtained with automated and conventional patch-clamp

Blocker	Chemical structure	IC_{50} conventional (μM)	IC_{50} automated (μM)	IC_{50} literature (μM)	Reference
Mibefradil	phenylalkylamine	0.50 ± 0.05	0.41 ± 0.06	0.27 ± 0.03	(Martin et al. 2000)
Verapamil	phenylalkylamine	20.2 ± 1.0	28.7 ± 3.8	21.4	(Freeze et al. 2006)
Flunarizine	diphenylpiperazine	1.02 ± 0.10	3.11 ± 0.95	0.53 ± 0.11	(Santi et al. 2002)
Ethosuximide	pyrrolidine	8.83 ± 0.43 ($\times 10^3$)	7.45 ± 0.42 ($\times 10^3$)	14 ± 3.7 ($\times 10^3$)	(Todorovic et al. 2000)
Clozapine	dibenzodiazepine	20.9 ± 0.7	18.8 ± 2.1	23.7 ± 1.3	(Choi and Rhim 2010)
1-Octanol	aliphatic alcohol	198 ± 10	217 ± 25	160 ± 13	(Todorovic et al. 2000)
Astemizole	piperadine	0.59 ± 0.07	0.76 ± 0.05	N/A	N/A
Nickel	divalent metal	121 ± 11	124 ± 11	250 ± 22	(Lee et al. 1999)[a]

All reference studies were performed in HEK293 cells. [a] 10 mM Ba^{2+} was used as a charge carrier in Lee et al. 2 mM Ca^{2+} was used in all other references.

nels were studied from whole-cell currents evoked by the test pulses of –20 mV for 50 ms at a holding potential of –100 mV. On average, 1 μM mibefradil inhibited the peak currents of $Ca_v3.1$ channels by 63 ± 4% (n = 5). Five concentrations of mibefradil (0.001 μM to 10 μM) were applied to the patched cells in a cumulative fashion as shown in the representative time trace of the peak currents of $Ca_v3.1$ channels in Fig. 1A.

Further pharmacological studies on $Ca_v3.1$ channels were carried out using the chemically diverse drugs known to block T-type calcium channels (see Supplementary material, Fig. S1). The inhibition of $Ca_v3.1$ peak currents by all of the examined blockers was concentration-dependent (Fig. 1B). Normalized peak current amplitudes in the presence of each drug were plotted as a function of drug concentration and fitted to a Hill equation. The concentration required for 50% inhibition (IC_{50}) was summarized in Table 1. For comparison, the IC_{50} values of each drug for $Ca_v3.1$ channels were also obtained using conventional patch-clamp (see Supplementary material, Fig. S2), which exhibited the similar values to those obtained with automated patch-clamp (Table 1). Overall, pharmacological data showed a good agreement between the two methods; a correlation coefficient (R) of 0.82 and a slope of 0.96 ± 0.05 were determined by a linear regression (open circles and solid line in Fig. 1C). A decent correlation was also observed in the comparison between the automated patch-clamp results and the reported values; R of 0.70 and a slope of 0.85 ± 0.09 (filled squares and dashed line in Fig. 1C).

For pharmacological studies of $Ca_v3.1$ channels with automated patch-clamp, the sealing rate was good (>80%); gigaseals onto the cell were mostly formed once the cells were attached (Fig. 2A). However, the rate for obtaining the whole-cell configuration was reduced to 43% with the mean initial membrane resistance (R_{wc}) of 1.66 ± 0.12 GΩ (median value of 710 MΩ, n = 390, Fig. 2B). The overall success rate of getting usable recordings was further dropped to 16% partly due to lack of functional channel expression, which is evident in the mean peak amplitude of $Ca_v3.1$ channel currents of –169 ± 7 pA (median value of –130 pA, n = 395), ranged from –20 to –1160 pA (Fig. 2C).

For the past five years, the developments of automated patch-clamp electrophysiology have been widely adapted in drug discovery (for reviews see Dunlop et al. 2008). The number of papers on ion channel studies using automated patch-clamp have been rapidly accumulated, where most studies compare the potencies of blockers and/or agonists obtained from automated patch-clamp to the values measured with conventional one, showing a good agreement.

T-type calcium channel specific drugs for clinical use need to be developed in a timely fashion, in which higher-throughput screening with automated patch-clamp techniques is necessary. The automated patch-clamp studies on T-type calcium channels would thus provide the valuable data for usage of an automated patch-clamp platform for such drug discovery. T-type calcium channels were previously studied with recombinant $Ca_v3.2$ T-type calcium channels using automated patch-clamp for the basic biophysical properties (Mathes et al. 2009), but this study did not provide pharmacological data. To rigorously characterize pharmacological properties of T-type calcium channels with automated patch-clamp, we focused on $Ca_v3.1$ channels, one of the three isoforms of T-type calcium channels. Various blockers with diverse chemical structures were tested against $Ca_v3.1$ channels to validate the ability of automated patch-clamp for ranking the drug potencies. The IC_{50} values obtained with automated patch-clamp are in good agreement with those determined with conventional patch-clamp (R of 0.82) as well as the published data (R of 0.70). A better correlation was observed with the values obtained in the present study than with the previously reported values, which is probably due to the differences in experimental conditions such as recording solutions and voltage protocols. The underestimated

IC_{50} values previously often observed due to the limited time for solution exchange and the adsorption of lipophilic test compounds (Guo and Guthrie 2005; Sorota et al. 2005) were not observed in the present work. Also, the range of the IC_{50} values extends over six orders of magnitude of concentrations with a slope of 0.96 determined by a linear regression, close to the unity line, indicating that the dynamic range of this method is broad enough for most of the test compounds to fall into this range. Thus, our pharmacological data with various drugs suggest that T-type calcium channels could be well studied using automated patch-clamp in a fast and reliable fashion.

The experimental throughput of an automated patch-clamp method has been reported to be increased by 5- to 45-fold over conventional patch-clamp (Brown 2009; Friis et al. 2009; Mathes et al. 2009). In the present work, the automated patch-clamp increases throughput of roughly 4-fold compared to conventional patch-clamp mainly due to the relatively low overall success rate of getting usable patches in $Ca_v3.1$ channel recordings, which could be a potential drawback for screening purposes. In contrast to conventional patch-clamp, where cells are manually selected for patch-clamping, cell selection is random in automated patch-clamp recordings. The low overall success rate may thus be partly caused by the small size of cells randomly selected, leading to the reduced current amplitudes. This problem could be solved by generating improved recombinant cell lines. Other cell lines such as Chinese hamster ovary (CHO) cells rather than HEK293 cells may express sufficiently measurable currents, thus being more compatible and robust with automated patch-clamp experiments (Clare et al. 2009). Indeed, the overall success rates in automated patch-clamp mainly depend on the combination of the cell line chosen and ion channels expressed, and CHO cells have been suggested to be a better choice than HEK293 cells to obtain the high success rates in automated patch-clamp experiments (Dunlop et al. 2008; Mathes et al. 2009). Another way to maximize the current amplitude is to optimize the cell preparation conditions and/or to change the composition of the patch solutions (Balasubramanian et al. 2009; Mathes et al. 2009). Using non-enzymatic cell dissociation solutions instead of trypsin for cell detachment may be less harsh on cells, thus

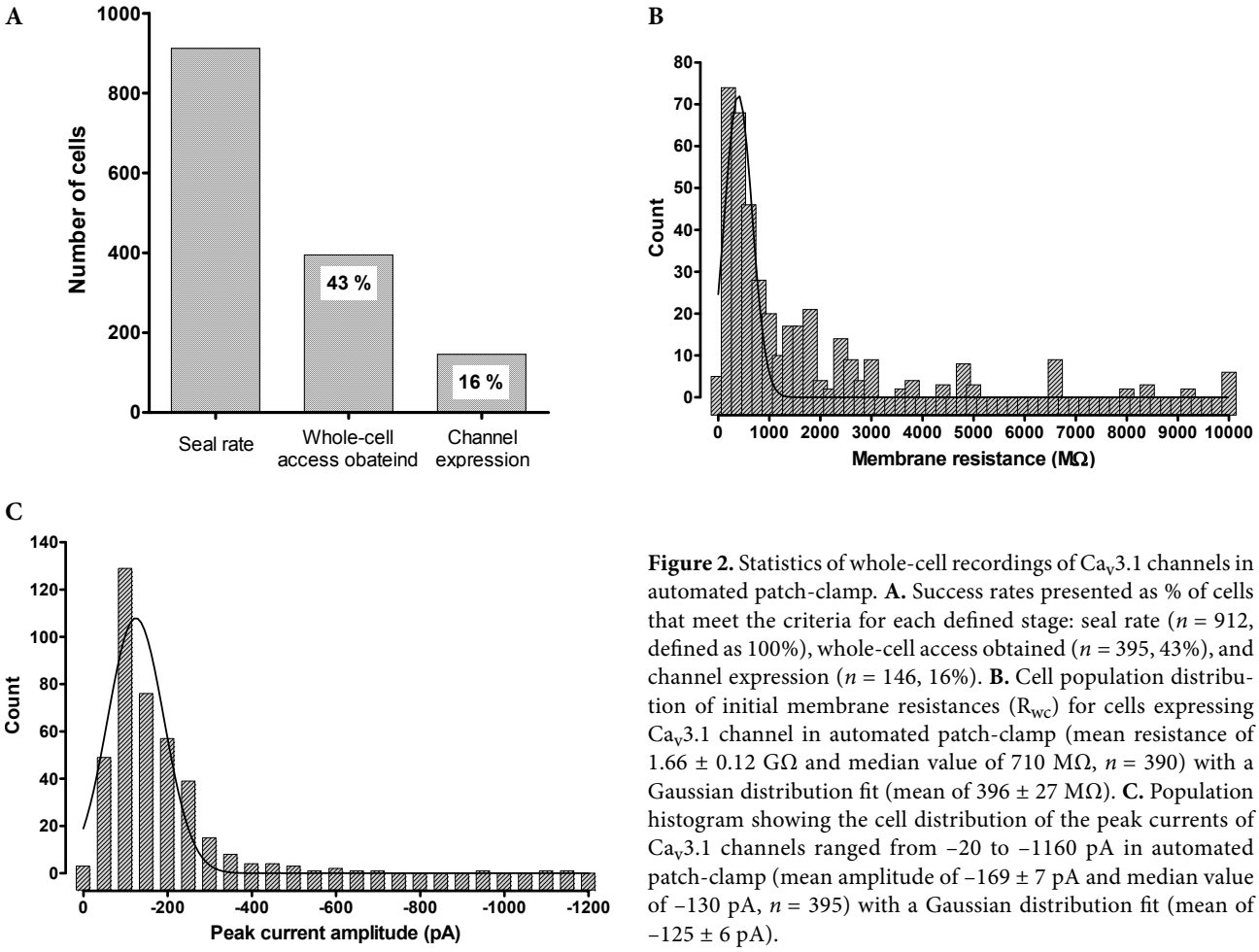

Figure 2. Statistics of whole-cell recordings of $Ca_v3.1$ channels in automated patch-clamp. **A.** Success rates presented as % of cells that meet the criteria for each defined stage: seal rate (n = 912, defined as 100%), whole-cell access obtained (n = 395, 43%), and channel expression (n = 146, 16%). **B.** Cell population distribution of initial membrane resistances (R_{wc}) for cells expressing $Ca_v3.1$ channel in automated patch-clamp (mean resistance of 1.66 ± 0.12 GΩ and median value of 710 MΩ, n = 390) with a Gaussian distribution fit (mean of 396 ± 27 MΩ). **C.** Population histogram showing the cell distribution of the peak currents of $Ca_v3.1$ channels ranged from –20 to –1160 pA in automated patch-clamp (mean amplitude of –169 ± 7 pA and median value of –130 pA, n = 395) with a Gaussian distribution fit (mean of –125 ± 6 pA).

enhancing channel currents since proteases could affect the current amplitudes (Rajamani et al. 2006). Modifying the composition of recording solutions, for example, adding cAMP into the intracellular solution may increase calcium currents because it has been known that PKA (cAMP-dependent protein kinase A)-mediated phosphorylation of $Ca_v3.1$ T-type calcium channels stimulates channel activity (Chemin et al. 2007), thus supposedly inducing enhancement in calcium currents.

In conclusion, the present work demonstrates that blockers of T-type calcium channels can be screened more efficiently and reliably using automated patch-clamp techniques. Drug potencies of T-type calcium channels obtained with both automated and conventional methods were similar, which is an important and useful feature for drug screening. Overall, given the significance of T-type calcium channels as drug targets, automated patch-clamp recordings of $Ca_v3.1$ channels could provide an alternative way for higher-throughput screening for novel drug discovery targeted against T-type calcium channels.

Acknowledgements. The authors declare no competing financial interests. This work was supported by KIST (2E21610), Mid-Career Researcher Program (20100000343), Pioneer Program (20100002215), and BRC of the 21st Century Frontier Research Program (2010K000813) from MEST, Korea.

References

Anderson M. P., Mochizuki T., Xie J., Fischler W., Manger J. P., Talley E. M., Scammell T. E., Tonegawa S. (2005): Thalamic Cav3.1 T-type Ca2+ channel plays a crucial role in stabilizing sleep. Proc. Natl. Acad. Sci. U.S.A. **102,** 1743–1748 doi:10.1073/pnas.0409644102

Balasubramanian B., Imredy J. P., Kim D., Penniman J., Lagrutta A., Salata J. J. (2009): Optimization of Ca(v)1.2 screening with an automated planar patch clamp platform. J. Pharmacol. Toxicol. Methods **59,** 62–72 doi:10.1016/j.vascn.2009.02.002

Bridgland-Taylor M. H., Hargreaves A. C., Easter A., Orme A., Henthorn D. C., Ding M., Davis A. M., Small B. G., Heapy C. G., Abi-Gerges N., Persson F., Jacobson I., Sullivan M., Albertson N., Hammond T. G., Sullivan E., Valentin J. P., Pollard C. E. (2006): Optimisation and validation of a medium-throughput electrophysiology-based hERG assay using IonWorks HT. J. Pharmacol. Toxicol. Methods **54,** 189–199 doi:10.1016/j.vascn.2006.02.003

Brown A. M. (2009): High throughput functional screening of an ion channel library for drug safety and efficacy. Eur. Biophys. J. **38,** 273–278 doi:10.1007/s00249-008-0356-2

Chemin J., Mezghrani A., Bidaud I., Dupasquier S., Marger F., Barrere C., Nargeot J., Lory P. (2007): Temperature-dependent modulation of CaV3 T-type calcium channels by protein kinases C and A in mammalian cells. J. Biol. Chem. **282,** 32710–32718 doi:10.1074/jbc.M702746200

Choi K. H., Rhim H. (2010): Inhibition of recombinant Ca(v)3.1 (alpha(1G)) T-type calcium channels by the antipsychotic drug clozapine. Eur. J. Pharmacol. **626,** 123–130 doi:10.1016/j.ejphar.2009.09.035

Clare J. J., Chen M. X., Downie D. L., Trezise D. J., Powell A. J. (2009): Use of planar array electrophysiology for the development of robust ion channel cell lines. Comb. Chem. High Throughput Screen **12,** 96–106 doi:10.2174/138620709787048000

Clozel J. P., Veniant M., Osterrieder W. (1990): The structurally novel Ca2+ channel blocker Ro 40-5967, which binds to the [3H] desmethoxyverapamil receptor, is devoid of the negative inotropic effects of verapamil in normal and failing rat hearts. Cardiovasc. Drugs Ther. **4,** 731–736 doi:10.1007/BF01856562

Dunlop J., Bowlby M., Peri R., Vasilyev D., Arias R. (2008): High-throughput electrophysiology: an emerging paradigm for ion-channel screening and physiology. Nat. Rev. Drug Discov. **7,** 358–368 doi:10.1038/nrd2552

Flatters S. J. L. (2005): T-type calcium channels: a potential target for the treatment of chronic pain. Drugs Fut. **30,** 573–580 doi:10.1358/dof.2005.030.06.915728

Freeze B. S., McNulty M. M., Hanck D. A. (2006): State-dependent verapamil block of the cloned human Ca(v)3.1 T-type Ca(2+) channel. Mol. Pharmacol. **70,** 718–726 doi:10.1124/mol.106.023473

Friis S., Mathes C., Sunesen M., Bowlby M. R., Dunlop J. (2009): Characterization of compounds on nicotinic acetylcholine receptor alpha7 channels using higher throughput electrophysiology. J. Neurosci. Methods **177,** 142–148 doi:10.1016/j.jneumeth.2008.10.007

Guo L., Guthrie H. (2005): Automated electrophysiology in the preclinical evaluation of drugs for potential QT prolongation. J. Pharmacol. Toxicol. Methods **52,** 123–135 doi:10.1016/j.vascn.2005.04.002

Khosravani H., Bladen C., Parker D. B., Snutch T. P., McRory J. E., Zamponi G. W. (2005): Effects of Cav3.2 channel mutations linked to idiopathic generalized epilepsy. Ann. Neurol. **57,** 745–749 doi:10.1002/ana.20458

Kim D., Park D., Choi S., Lee S., Sun M., Kim C., Shin H. S. (2003): Thalamic control of visceral nociception mediated by T-type Ca2+ channels. Science **302,** 117–119 doi:10.1126/science.1088886

Krayenbuhl J. C., Vozeh S., Kondo-Oestreicher M., Dayer P. (1999): Drug-drug interactions of new active substances: mibefradil example. Eur. J. Clin. Pharmacol. **55,** 559–565 doi:10.1007/s002280050673

Lee J. H., Gomora J. C., Cribbs L. L., Perez-Reyes E. (1999): Nickel block of three cloned T-type calcium channels: low concentrations selectively block alpha1H. Biophys. J. **77,** 3034–3042 doi:10.1016/S0006-3495(99)77134-1

Ly J. Q., Shyy G., Misner D. L. (2007): Assessing hERG channel inhibition using PatchXpress. Clin. Lab. Med. **27,** 201–208 doi:10.1016/j.cll.2006.12.011

Martin R. L., Lee J. H., Cribbs L. L., Perez-Reyes E., Hanck D. A. (2000): Mibefradil block of cloned T-type calcium channels. J. Pharmacol. Exp. Ther. **295,** 302–308

Mathes C., Friis S., Finley M., Liu Y. (2009): QPatch: the missing link between HTS and ion channel drug discovery. Comb. Chem. High Throughput Screen **12,** 78–95 doi:10.2174/138620709787047948

McCallum J. B., Kwok W. M., Mynlieff M., Bosnjak Z. J., Hogan Q. H. (2003): Loss of T-type calcium current in sensory neurons of rats with neuropathic pain. Anesthesiology **98,** 209–216 doi:10.1097/00000542-200301000-00032

Milligan C. J., Li J., Sukumar P., Majeed Y., Dallas M. L., English A., Emery P., Porter K. E., Smith A. M., McFadzean I., Beccano-Kelly D., Bahnasi Y., Cheong A., Naylor J., Zeng F., Liu X., Gamper N., Jiang L. H., Pearson H. A., Peers C., Robertson B., Beech D. J. (2009): Robotic multiwell planar patch-clamp for native and primary mammalian cells. Nat. Protoc. **4,** 244–255 doi:10.1038/nprot.2008.230

Perez-Reyes E. (2003): Molecular physiology of low-voltage-activated t-type calcium channels. Physiol. Rev. **83,** 117–161

Rajamani S., Anderson C. L., Valdivia C. R., Eckhardt L. L., Foell J. D., Robertson G. A., Kamp T. J., Makielski J. C., Anson B. D., January C. T. (2006): Specific serine proteases selectively damage KCNH2 (hERG1) potassium channels and I(Kr). Am. J. Physiol. Heart Circ. Physiol. **290,** H1278–1288 doi:10.1152/ajpheart.00777.2005

Santi C. M., Cayabyab F. S., Sutton K. G., McRory J. E., Mezeyova J., Hamming K. S., Parker D., Stea A., Snutch T. P. (2002): Differential inhibition of T-type calcium channels by neuroleptics. J. Neurosci. **22,** 396–403

Sorota S., Zhang X. S., Margulis M., Tucker K., Priestley T. (2005): Characterization of a hERG screen using the IonWorks HT: comparison to a hERG rubidium efflux screen. Assay Drug. Dev. Technol. **3,** 47–57 doi:10.1089/adt.2005.3.47

Todorovic S. M., Perez-Reyes E., Lingle C. J. (2000): Anticonvulsants but not general anesthetics have differential blocking effects on different T-type current variants. Mol. Pharmacol. **58,** 98–108

Tsakiridou E., Bertollini L., de Curtis M., Avanzini G., Pape H. C. (1995): Selective increase in T-type calcium conductance of reticular thalamic neurons in a rat model of absence epilepsy. J. Neurosci. **15,** 3110–3117

Vitko I., Chen Y., Arias J. M., Shen Y., Wu X. R., Perez-Reyes E. (2005): Functional characterization and neuronal modeling of the effects of childhood absence epilepsy variants of CACNA1H, a T-type calcium channel. J. Neurosci. **25,** 4844–4855 doi:10.1523/JNEUROSCI.0847-05.2005

Received: August 20, 2010
Final version accepted: November 26, 2010

Supplementary Material

Pharmacological studies of $Ca_V3.1$ T-type calcium channels using automated patch-clamp techniques

Kee-Hyun Choi, Chiman Song, Chan S. Cheong and Hyewhon Rhim

Life/Health Division, Korea Institute of Science and Technology, 39-1 Hawolgok-Dong, Seongbuk-Gu, Seoul 136-791, Korea

Supplementary Materials and Methods

Cell culture and preparation

Human embryonic kidney 293 (HEK293) cells stably expressing human $Ca_v3.1$ T-type calcium channels along with the Kir2.1 inward rectifier potassium channels were obtained from the Korea Research Institute of Bioscience and Biotechnology. Since inward rectifier potassium channels lower the resting membrane potential, the HEK293 cell line coexpressing inward rectifier potassium channels was used to prevent cell damage due to the unwanted calcium influx during cell culture (Balasubramanian et al. 2009). Cells were cultured in Dulbecco's modified Eagle's medium containing 10% (v/v) fetal bovine serum, penicillin (100 U/ml) and streptomycin (100 μg/ml) as well as selection antibiotics, geneticin G418 (200 μg/ml) for α_{1G} and puromycin (1 μg/ml) for Kir2.1 in humidified 5% CO_2 at 37°C. Cells were passaged every three days by treatment with trypsin-EDTA. For automated patch-clamp recordings, cells were plated into the 100-mm culture dishes. Cells at 50–80% confluency were harvested by treatment with trypsin-EDTA, washed twice and resuspended in the extracellular solution at a final cell density of $1–5 \times 10^6$ cells/ml. For conventional patch-clamp recordings, cells were seeded onto the poly-L-lysine coated glass cover slips. Whole-cell patch-clamp experiments were carried out 24–48 h after seeding.

Automated patch-clamp electrophysiology

The automated patch-clamp device, NPC-16 Patchliner (Nanion Technologies, Germany) was used for whole-cell recordings. Whole-cell currents were recorded with the intracellular solution containing (in mM): 50 KCl, 60 KF, 10 NaCl, 2 $MgCl_2$, 20 EGTA and 10 HEPES (pH 7.2) and with the extracellular solution containing (in mM): 140 NaCl, 4 KCl, 5 glucose, 2 $CaCl_2$, 1 $MgCl_2$ and 10 HEPES (pH 7.4) (Milligan et al. 2009). To assist stable seal formations, the seal enhancer containing (in mM): 80 NaCl, 3 KCl, 35 $CaCl_2$, 10 $MgCl_2$ and 10 HEPES (pH 7.4) was used only at the seal formation step. Prior to whole-cell recordings, the external solution containing the seal enhancer was exchanged for the extracellular solution described above. Channel currents were recorded by the parallel EPC-10 patch-clamp amplifiers (HEKA Elektronik, Germany) and low-pass filtered (10 kHz) with a 4-pole Bessel filter. Cell suspension and patch solutions were automatically added onto the four recording wells in the microfabricated disposable chip (NPC-16 Chip, Nanion Technologies, Germany). Each test compound (40 μl) was applied to the patch-clamped cells via four pipette tips of NPC-16 Patchliner with a speed of 4 μl/s. Astemizole was purchased from Wako Pure Chemical Industries Ltd. (Osaka, Japan). All other chemicals were obtained from Sigma-Aldrich Corp. (St. Louis, MO, USA).

Conventional patch-clamp electrophysiology

Micropipettes were pulled from borosilicate glass capillaries (GC150T-7.5; Warner Instrument Corp., Hamden, CT, USA) on a puller (P-97; Sutter Instrument Co., Novato, CA, USA) with resistance of ~3 MΩ. Whole-cell currents were recorded with the same intracellular and extracellular solutions used for automated patch-clamp without seal enhancer. Whole-cell recordings were performed at room temperature with an EPC-10 patch-clamp amplifier (HEKA Elektronik, Germany) and low-pass filtered (10 kHz) with a 4-pole Bessel filter. Whole-cell currents were acquired and digitized at 20 kHz using the Patchmaster (HEKA Elektronik, Germany).

Data analysis

Whole-cell recordings were analyzed using the Patchmaster/Fitmaster, IGOR Pro (WaveMetrics Inc., Portland, OR, USA), and the GraphPad Prism 4 (GraphPad Software, Inc., La Jolla, CA, USA) software.

Corresponding author e-mail: keehyun@kist.re.kr; hrhim@kist.re.kr

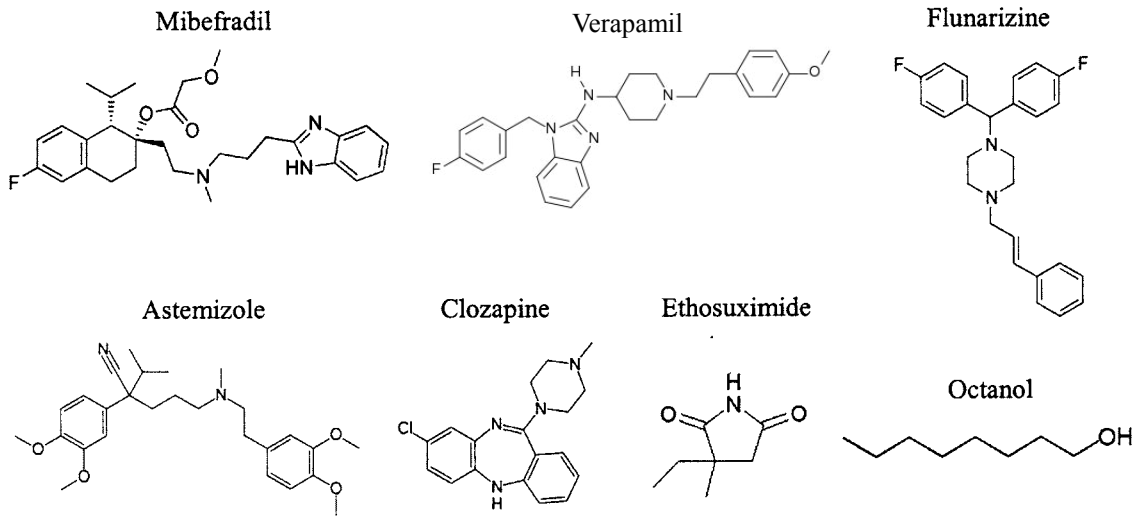

Figure S1. Structures of known T-type calcium channel blockers.

The dose-response curve was fitted to a Hill equation (sigmoidal dose-response equation),

$$I = I_{min} + (I_{max} - I_{min}) / (1 + 10^{((LogIC50 - C) \times h)}) \quad (S1)$$

where I_{min} and I_{max} are the normalized minimum and maximum currents, respectively. IC_{50} is the half-maximum inhibition concentration. C is the logarithm of concentration and h is the Hill coefficient.

The curve for steady-state activation was fitted to a Boltzmann sigmoidal equation

$$G = G_{min} + (G_{max} - G_{min}) / (1 + \exp((V_{1/2\text{-act}} - V) / slope_{act})) \quad (S2)$$

where G_{min} and G_{max} are the normalized minimum and maximum conductance, respectively. $V_{1/2\text{-act}}$ is the mean potential for half-activation and $slope_{act}$ is the slope activation factor.

The curve for steady-state inactivation was also fitted to a Boltzmann sigmoidal equation

$$I = I_{min} + (I_{max} - I_{min}) / (1 + \exp((V_{1/2\text{-inact}} - V) / slope_{inact})) \quad (S3)$$

where I_{min} and I_{max} are the normalized minimum and maximum currents, respectively. $V_{1/2\text{-inact}}$ is the mean potential for half-inactivation and $slope_{inact}$ is the slope inactivation factor.

Recovery kinetics were fitted to a double-exponential association equation

$$\% \text{ Recovery} = amp_f(1 - \exp(t / k_f)) + amp_s(1 - \exp(t / k_s)) \quad (S4)$$

where *amp* is the relative amplitude, t is the time and k is the rate constant. f and s represent the fast and the slow components, respectively. The time constant (τ) is 0.69 / k.

The significance of observed differences was evaluated by an ANOVA test. A p value of <0.05 was considered statistically significant. All results are presented as the means ± S.E.M.

Supplementary Results

Biophysical properties of $Ca_v3.1$ T-type calcium channels in automated patch-clamp were examined in a current-voltage (I-V) relationship by 50-ms test pulses from –90 to +50 mV in 5 mV-increments at a holding potential of –100 mV (Fig. S3A). The peak currents were normalized to the maximum peak currents and presented in normalized I (Fig. S3B). The maximum peak currents in an I-V curve were occurred when cells were stimulated by a test pulse of –20 mV (n = 24). To examine steady-state activation properties, the channel activation curve was generated by converting currents in an I-V curve to the conductance (G) and normalizing to the maximum conductance (G / G_{max}), and fitted to a Boltzmann sigmoidal function (Fig. S3C). The activation of $Ca_v3.1$ channels shows the mean potential for half-activation ($V_{1/2\text{-act}}$) of –31 ± 1 mV and the slope activation factor ($slope_{act}$) of 6.1 ± 0.4 (n = 20).

To further elucidate the biophysical properties of $Ca_v3.1$ channels, steady-state inactivation of $Ca_v3.1$ channels was determined. A steady-state inactivation curve was obtained by applying a 2-s prepulse to various potentials from –105 to –40 mV and a test pulse to –20 mV at a holding potential of –100 mV (Fig. S4A). The peak currents were normalized

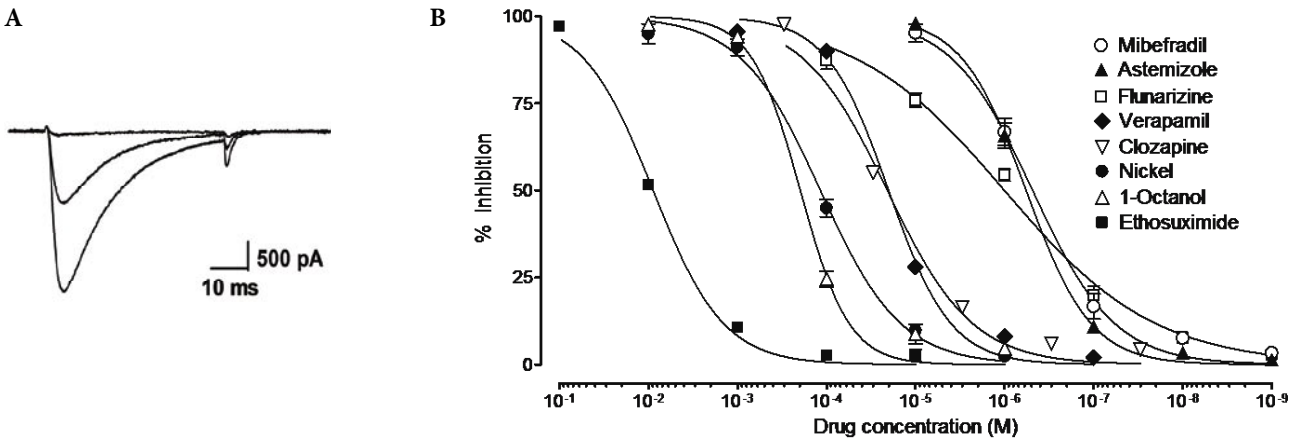

Figure S2. Pharmacological characterization of $Ca_v3.1$ channels with conventional patch-clamp. **A.** Representative whole-cell recording of $Ca_v3.1$ channels evoked by 50-ms test pulses to –20 mV at a holding potential of –100 mV. Whole-cell currents of $Ca_v3.1$ channels were blocked by ~60% on average upon applying 1 μM mibefradil to the bath solution (control, 1 μM and 10 μM of mibefradil applied). **B.** Dose-response curves of drug inhibition of the peak $Ca_v3.1$ currents presented as percent inhibition (% inhibition) as a function of drug concentration: mibefradil (○), astemizole (▲), flunarizine (□), verapamil (◆), clozapine (▽), nickel (●), 1-octanol (△) and ethosuximide (■). Each point is pooled from at least five recordings. The curves were fitted to a Hill equation to obtain the IC_{50} values, summarized in Table 1. Error bars represent S.E.M.

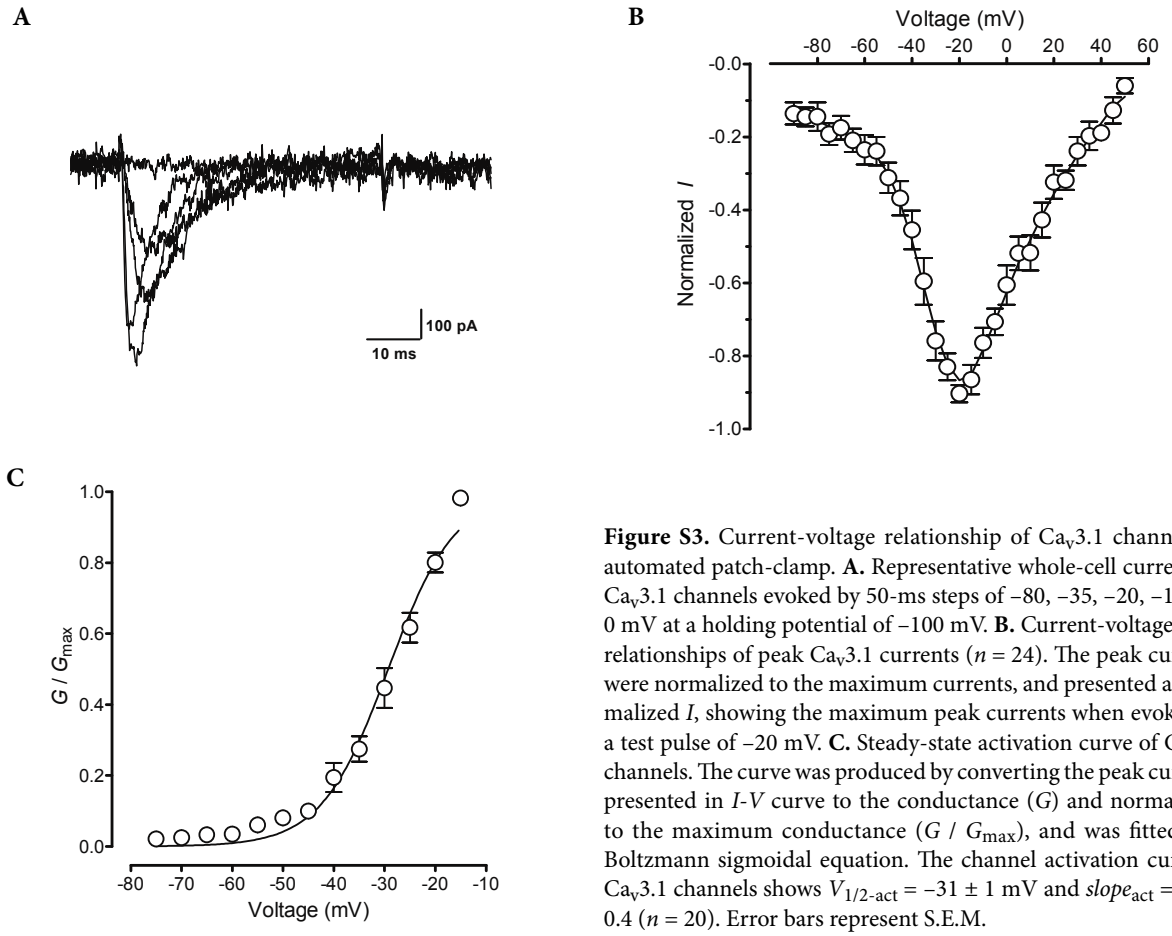

Figure S3. Current-voltage relationship of $Ca_v3.1$ channels in automated patch-clamp. **A.** Representative whole-cell currents of $Ca_v3.1$ channels evoked by 50-ms steps of –80, –35, –20, –15 and 0 mV at a holding potential of –100 mV. **B.** Current-voltage (*I-V*) relationships of peak $Ca_v3.1$ currents (n = 24). The peak currents were normalized to the maximum currents, and presented as normalized *I*, showing the maximum peak currents when evoked by a test pulse of –20 mV. **C.** Steady-state activation curve of $Ca_v3.1$ channels. The curve was produced by converting the peak currents presented in *I-V* curve to the conductance (*G*) and normalizing to the maximum conductance (G / G_{max}), and was fitted to a Boltzmann sigmoidal equation. The channel activation curve of $Ca_v3.1$ channels shows $V_{1/2\text{-act}}$ = –31 ± 1 mV and $slope_{act}$ = 6.1 ± 0.4 (n = 20). Error bars represent S.E.M.

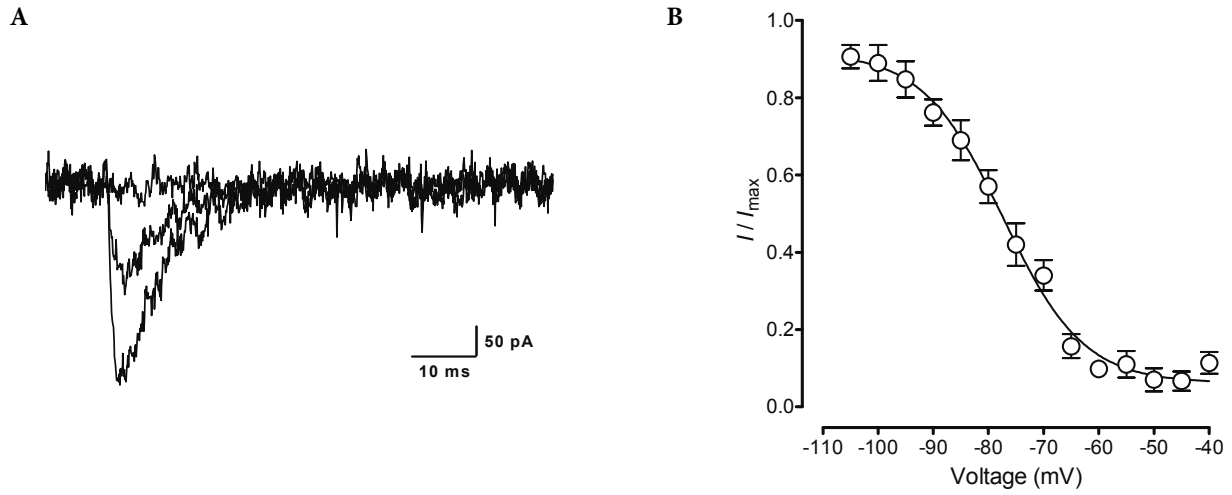

Figure S4. Steady-state inactivation properties of $Ca_v3.1$ channels in automated patch-clamp. **A.** Representative whole-cell currents of $Ca_v3.1$ channels evoked by a 50-ms step to –20 mV from a holding potential of –100 mV after 2-s pre-depolarization pulses of –110, –75 and –40 mV. **B.** Steady-state inactivation curve of $Ca_v3.1$ channels. The curve was generated by normalizing to the maximum currents (I/ I_{max}) and presenting as a function of pre-depolarization potentials, and was fitted to a Boltzmann sigmoidal equation. The steady-state inactivation curve has $V_{1/2\text{-inact}}$ = –79 ± 1 mV and $slope_{inact}$ = 8.6 ± 0.7 (n = 16). Error bars represent S.E.M.

to the maximum peak currents (I / I_{max}), and the channel inactivation curve was fitted to a Boltzmann sigmoidal equation (Fig. S4B). The mean potential of half-inactivation ($V_{1/2\text{-inact}}$) and the slope inactivation factor in steady-state inactivation curve ($slope_{inact}$) for $Ca_v3.1$ channels were –79 ± 1 mV and 8.6 ± 0.7, respectively (n = 16). Steady-state inactivation properties of $Ca_v3.1$ channels were further examined by observing recovery from steady-state inactivation. In the recovery experiments, cells were inactivated by steps to –20 mV for 50 ms, and then tested by 50-ms steps to –20 mV with 0, 10, 20, 40, 80, 160, 320, 640, 1280 and 2560-ms intervals (Fig. S5A). To analyze recovery kinetics,

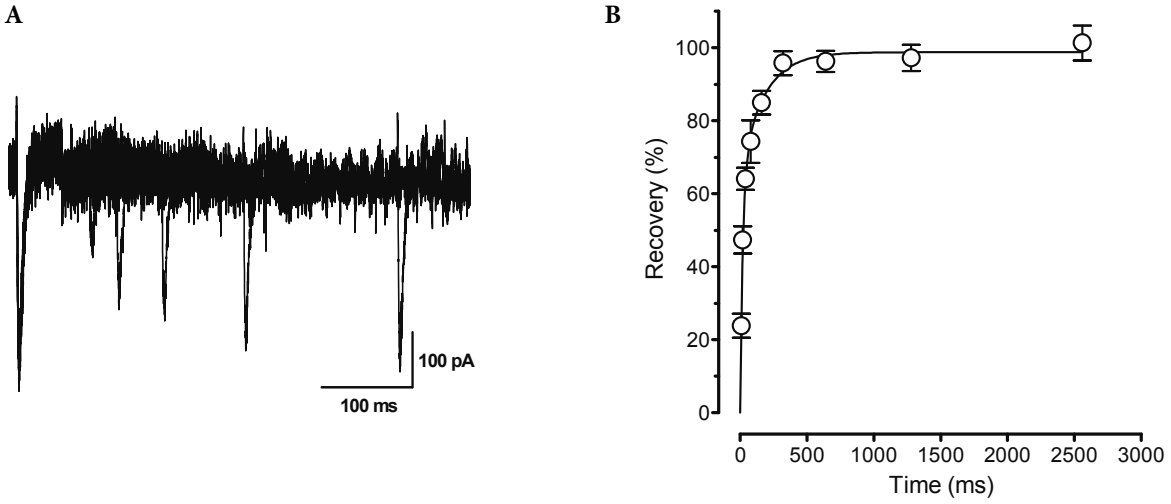

Figure S5. Recovery from steady-state inactivation of $Ca_v3.1$ channels in automated patch-clamp. **A.** Representative whole-cell current traces of $Ca_v3.1$ channels evoked by 50-ms steps of –20 mV with intervals of 10, 20, 40, 80, 160, and 320 ms after 50-ms pre-pulses of –20 mV. **B.** Percent recovery (% Recovery) from the steady-state inactivation (n = 11). The time course of recovery from the steady-state inactivation was fitted to a double-exponential function. The time constants and the relative amplitudes of the slow (τ_s and amp_s) and the fast components (τ_f and amp_f) in recovery kinetics were 389 ± 156 ms, 34 ±10 and 24 ± 9 ms, 71 ± 9, respectively. Error bars represent S.E.M.

Table S1. Summary of the biophysical properties of $Ca_v3.1$ channels obtained with automated and conventional patch-clamp

	Parameter	Patch-clamp	
		Conventional	Automated
Current-voltage relationship	V_{max} (mV)	–30	–20
Steady-state activation	$V_{1/2\text{-act}}$ (mV)	–48 ± 1	–31 ± 1
	$slope_{act}$	4.9 ± 0.3	6.1 ± 0.4
Steady-state inactivation	$V_{1/2\text{-inact}}$ (mV)	–72 ± 2	–79 ± 1
	$slope_{inact}$	4.0 ± 0.1	8.6 ± 0.7
Recovery from inactivation	τ_s (ms) (amp_s)	153 ± 14 (23 ± 4)	389 ± 156 (34 ± 10)
	τ_f (ms) (amp_f)	20 ± 1 (77 ± 4)	24 ± 9 (71 ± 9)

V_{max}, the mean potential where maximum peak currents occur in the current-voltage curve; $V_{1/2\text{-act}}$, the mean potential for half-activation; $slope_{act}$, the slope activation factor; $V_{1/2\text{-inact}}$, the mean potential for half-inactivation; $slope_{inact}$, the slope inactivation factor; τ, the time constant; *amp*, the relative amplitude; *f* and *s,* the fast and the slow components.

the two kinetic components in recovery were obtained using a double-exponential fit (Fig. S5B). The slow component has a time constant (τ_s) of 389 ± 156 ms with a relative amplitude (amp_s) of 34 ± 10 while the fast component shows a time constant (τ_f) of 24 ± 9 ms with a relative amplitude (amp_f) of 71 ± 9 (n = 11 and Fig. S5B).

The biophysical parameters obtained with automated patch-clamp were compared with those determined with conventional patch-clamp (Figs. S6–S8), and summarized in Table S1. Inactivation properties $Ca_v3.1$ channels such as steady-state inactivation and recovery from steady-state inactivation were similar in both methods within the experi-

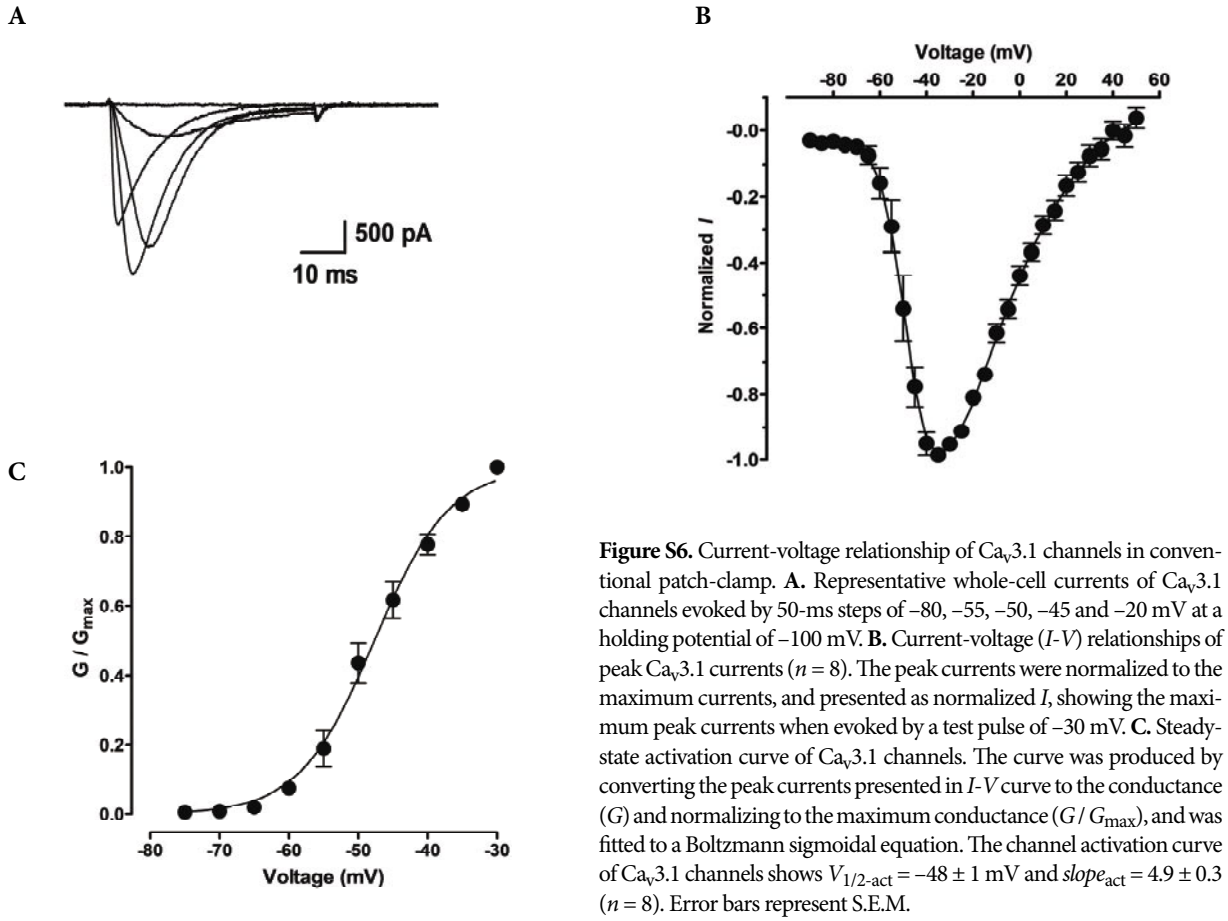

Figure S6. Current-voltage relationship of $Ca_v3.1$ channels in conventional patch-clamp. **A.** Representative whole-cell currents of $Ca_v3.1$ channels evoked by 50-ms steps of –80, –55, –50, –45 and –20 mV at a holding potential of –100 mV. **B.** Current-voltage (*I-V*) relationships of peak $Ca_v3.1$ currents (n = 8). The peak currents were normalized to the maximum currents, and presented as normalized *I*, showing the maximum peak currents when evoked by a test pulse of –30 mV. **C.** Steady-state activation curve of $Ca_v3.1$ channels. The curve was produced by converting the peak currents presented in *I-V* curve to the conductance (G) and normalizing to the maximum conductance (G / G_{max}), and was fitted to a Boltzmann sigmoidal equation. The channel activation curve of $Ca_v3.1$ channels shows $V_{1/2\text{-act}}$ = –48 ± 1 mV and $slope_{act}$ = 4.9 ± 0.3 (n = 8). Error bars represent S.E.M.

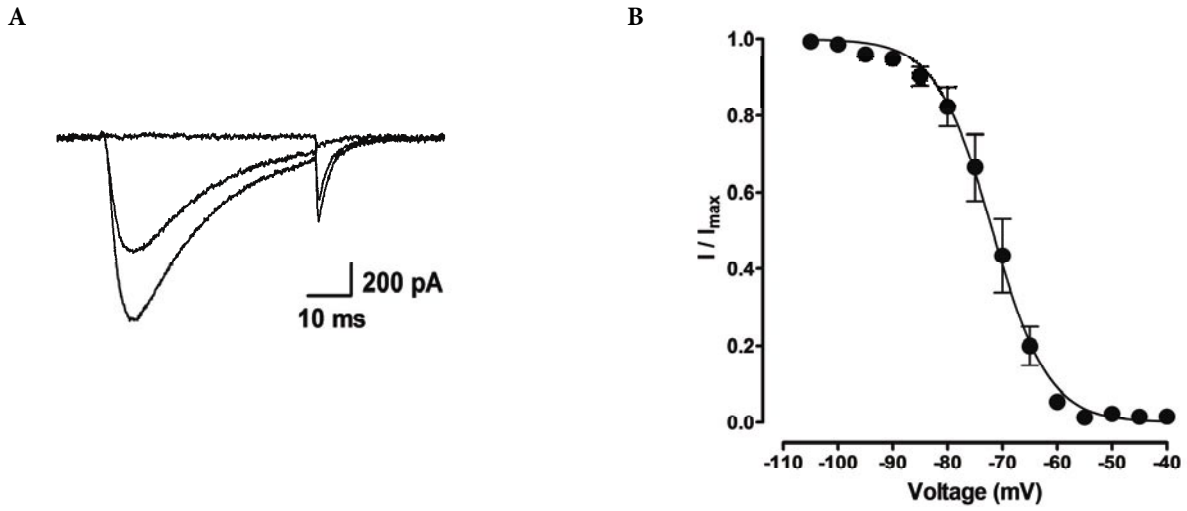

Figure S7. Steady-state inactivation properties of $Ca_v3.1$ channels in conventional patch-clamp. **A.** Representative whole-cell currents of $Ca_v3.1$ channels evoked by a 50-ms step to –20 mV from a holding potential of –100 mV after 2-s pre-depolarization pulses of –110, –70 and –40 mV. **B.** Steady-state inactivation curve of $Ca_v3.1$ channels. The curve was generated by normalizing to the maximum currents (I / I_{max}) and presenting as a function of pre-depolarization potentials, and was fitted to a Boltzmann sigmoidal equation. The steady-state inactivation curve has $V_{1/2\text{-inact}}$ = –72 ± 2 mV and $slope_{inact}$ = 4.0 ± 0.1 (n = 8). Error bars represent S.E.M.

mental error. A slight hyperpolarizing shift was observed in the steady-state inactivation curve obtained with automated patch-clamp when compared to the conventional method, but this difference was not statistically significant (two-way repeated-measures ANOVA test, p = 0.067). However, activation properties of $Ca_v3.1$ channels appeared to be different between automated and conventional patch-clamp studies even under the same experimental conditions; identical cell lines and patch solutions as well as pulse protocols were used in the both experiments. In particular, the mean potential where the maximum peak currents occur (V_{max}), and consequently the $V_{1/2\text{-act}}$ value obtained using automated

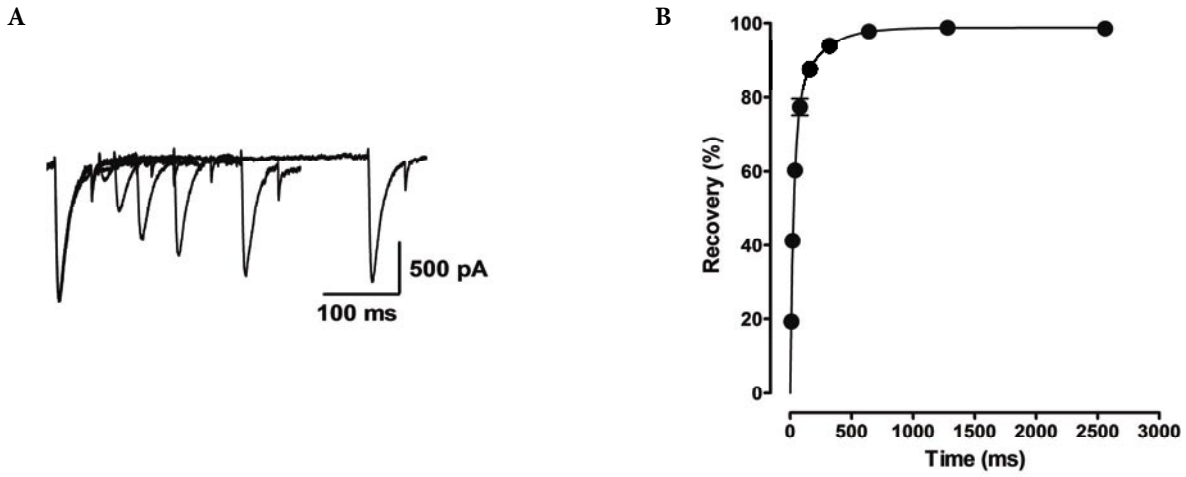

Figure S8. Recovery from steady-state inactivation of $Ca_v3.1$ channels in conventional patch-clamp. **A.** Representative whole-cell current traces of $Ca_v3.1$ channels evoked by 50-ms steps of –20 mV with intervals of 10, 20, 40, 80, 160 and 320 ms after 50-ms pre-pulses of –20 mV. **B.** Percent recovery (% recovery) from the steady-state inactivation (n = 9). The time course of recovery from the steady-state inactivation was fitted to a double-exponential function. The time constants and the relative amplitudes of the slow (τ_s and amp_s) and the fast components (τ_f and amp_f) in recovery kinetics were 153 ± 14 ms, 23 ± 4 and 20 ± 1 ms, 77 ± 4, respectively. Error bars represent S.E.M.

patch-clamp did not recapitulate the parameters determined using conventional patch-clamp (two-way repeated-measures ANOVA test, * $p < 0.05$ for IV curves, *** $p < 0.0001$ for steady-state activation curves). The mid-point of a steady-state activation curve was shifted to more positive potentials in automated patch-clamp.

Supplementary Discussion

An apparent depolarizing shift in a steady-state activation curve of $Ca_v3.1$ channels was observed with automated patch-clamp when compared to the conventional method. The observed discrepancies in biophysical parameters between the two methods might result in part from the relatively small currents of the cell line used in the present study, leading to the low signal-to-noise ratio. Analyzing the data with only higher amplitude currents in automated patch-clamp would be the best way to test whether the observed differences result from the different current amplitudes. However, almost all patches obtained from automated patch-clamp exhibit the currents less than ~400 pA as shown in Fig. 2C while conventional patch-clamp provides patches with the currents in the 1~2 nA range. Thus, it is practically challenging to obtain data that have comparable current amplitudes to conventional patch-clamp data from automated patch-clamp.

Other possibilities including the difference in the setup design might account for the observed differences in biophysical properties. In the conventional patch-clamp setup for the present study, the standard polyethylene tubing is used for perfusion while the automated patch-clamp setup has a stainless steel pipette tip for drug application. Since this rigid tip is not disposable, the only way to prevent any chance of contamination is an extensive wash. Although a thorough wash was carried out after each drug application, some sticky compounds might be adsorbed to the tip during pharmacological studies, and then be released while biophysical studies were performed, thereby affecting the steady-state activation properties of $Ca_v3.1$ channels. Another possible influence might come from the different cell conditions for patch-clamp recordings in each setup. For conventional patch-clamp recordings, cells are attached onto the poly-L-lysine coated glass cover while the automated patch-clamp setup is designed to use cell suspension. Suspended cells might exhibit different biophysical characteristics from surface-attached cells.

Most studies using automated patch-clamp have been focusing on pharmacological properties of ion channels for drug screening purposes while reports on biophysical characterization using automated patch-clamp are relatively limited. Activation properties of T-type calcium channels studied with recombinant $Ca_v3.2$ channels using automated patch-clamp were reported to be consistent with the values determined with conventional patch-clamp (Mathes et al. 2009). Interestingly, however, the different results between the conventional and automated patch-clamp systems were observed in biophysical properties of $Ca_v1.2$ L-type calcium channels (Balasubramanian et al. 2009). The automated patch-clamp setup did not recapitulate the steady-state activation and inactivation characteristics of $Ca_v1.2$ channels in the presence of L-type calcium channel selective agonist, BayK8644 determined in conventional patch-clamp. These discrepancies were attributed to possible changes to patch parameters such as resistance during biophysical characterization.

Overall, the detailed characterization of biophysical properties of T-type calcium channels with automated patch-clamp needs to be conducted with caution.

Supplementary References

Balasubramanian B., Imredy J. P., Kim D., Penniman J., Lagrutta A., Salata J. J. (2009): Optimization of Ca(v)1.2 screening with an automated planar patch clamp platform. J. Pharmacol. Toxicol. Methods **59,** 62–72
doi:10.1016/j.vascn.2009.02.002

Mathes C., Friis S., Finley M., Liu Y. (2009): QPatch: the missing link between HTS and ion channel drug discovery. Comb. Chem. High Throughput Screen **12,** 78–95
doi:10.2174/138620709787047948